CHAPTER 5

Colloidal CdSe QDs and PQT-12 Based Hybrid Self-Powered Photodetectors*

Contents

*Part of this work has been published as:

Hemant Kumar et al. “Colloidal CdSe Quantum Dots and PQT-12 Based Low-Temperature Self-Powered Hybrid Photodetector.” *IEEE Photonics Technology Letters*,29(20):1715-1718, 2017.

CHAPTER 5

Colloidal CdSe QDs and PQT-12 Based Hybrid Self-Powered Photodetectors

5.1 Introduction

In Chapter-4, we have investigated the optical and electrical characteristics of the self-powered PDs using colloidal QDs of inorganic semiconductors such as the CdSe and ZnO QDs. We have observed from the literature survey that hybrid PD using the combination of organic and inorganic semiconductors are of great interests to the researchers due to the possibility of exploring the intrinsic high carrier mobility and high absorption coefficient of inorganic semiconductor (Xie *et al.*, 2013; Game *et al.*, 2014; Bera *et al.*, 2016) and low-temperature processing feature of the organic semiconductors simultaneously for the performance improvement of such devices. In view of the above, we have investigated the electrical and optical characteristics of an Au/CdSe QDs/PQT-12/ITO based self-powered hybrid PD in the present chapter. The fabricated PD is illuminated from the backside to achieve 100% illumination area through the transparent ITO substrate. The ZnO QDs used in Chapter-4 has been replaced by the semiconducting polymer PQT-12 to reduce the device fabrication temperature from 250°C to 140°C. Two asymmetric depletion widths formed at PQT-12/CdSe and Au/CdSe junctions at two sides of the active CdSe QDs layer control the operation of the proposed detector. The layout of the chapter is given below:

Section 5.2 discusses the experimental details for the fabrication of hybrid self-powered PD under study. The effect of PQT-12 polymer on optical and electrical

properties of the Au/CdSe QDs based hybrid self-powered PD are discussed in details Section 5.3. Finally, the conclusion and summary of the present chapter have been presented in Section 5.4.

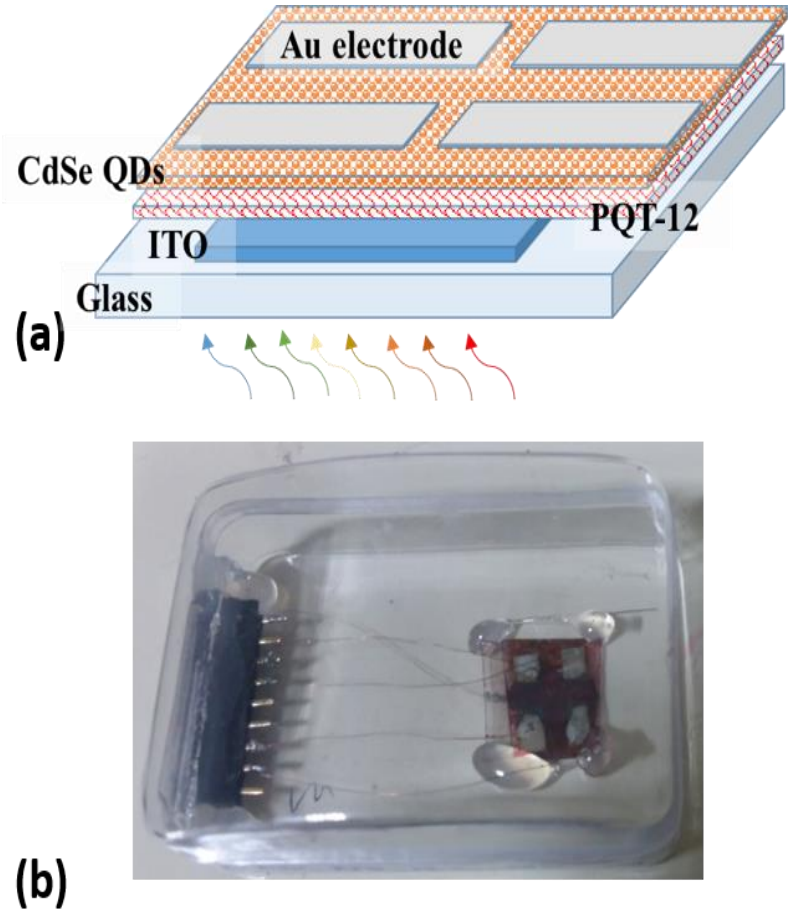

Figure 5.1: (a) Schematic device structure and (b) fabricated ITO/PQT-12/CdSe QDs/Au hybrid photodetector

5.2 Experimental Details

The proposed Au/CdSe QDs/PQT-12/ITO hybrid self-powered PD structure and the fabricated device is shown in Figure 5.1 (a) and (b) where the light coupled into the device from the back side to achieve the maximum illumination area of 100% (Baierl *et al.*, 2012). The front illumination is avoided since the opaque Au electrode may prevent a significant portion of the incident light from entering into the active layer of the

device in this case as discussed in chapter 4. However, the backside illumination allows a portion of the light passing through the active layer to get reflected back to it from the Au electrode layer. Thus, the back illumination increases the effective optical power density in the active region which in turn, improves the photodetection capability of the device (Y. Kumar, Kumar, Mukherjee, *et al.*, 2017). The ITO (work function: 4.7 eV) and Au (work function: 5.0 eV) have been used for the top and bottom electrode contacts of the device respectively. The energy band diagram of the complete device is shown in Figure 5.2 (b).

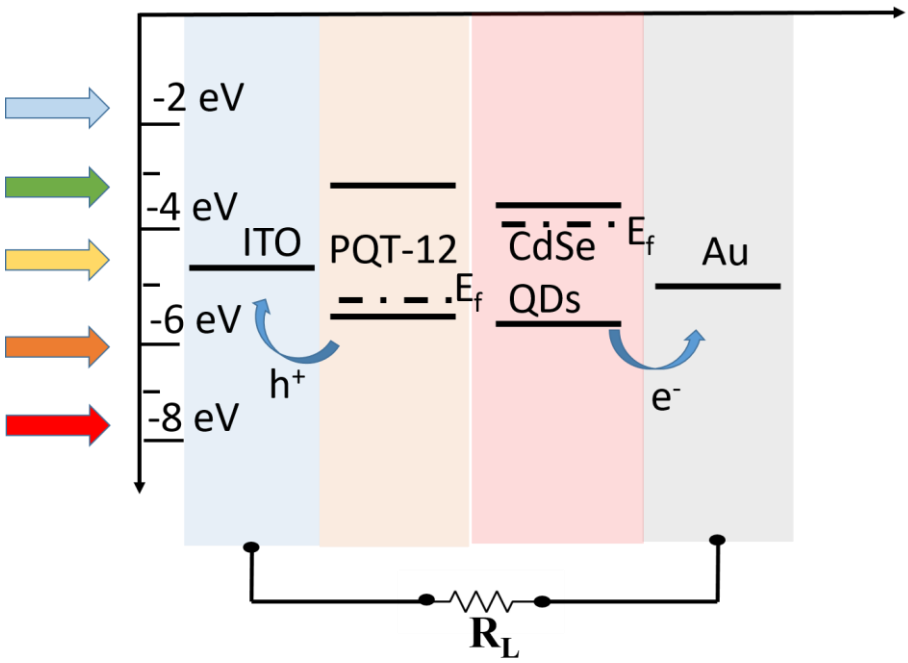

Figure 5.2: Schematic energy band diagram at thermal equilibrium.

The ITO forms a nearly ohmic junction with the PQT-12 (Pandey *et al.*, 2015) of electron affinity *(*χ~5.24 eV*)* and bandgap *(*E_g*~2.27* eV) (Ong *et al.*, 2005). Au forms a Schottky junction with CdSe QDs with electron affinity and bandgap of 4.3 eV and 2.2 eV respectively (Oertel *et al.*, 2005). The CdSe QDs active layer is assumed to be fully depleted by two depletion regions at Au/CdSe and PQT-12/CdSe junctions to control the operation of hybrid PD structure.

5.2.1 Device Fabrication

The ITO substrates (15×15 mm^2) are thoroughly cleaned by the method as reported in (Y. Kumar, Kumar, Rawat, *et al.*, 2017). The PQT-12 solution is deposited on the ITO substrate by repeated drop casting for five times to achieve very high thickness and then by spin-coating technique (SPM-150LC, GmbH). Spin coating is performed at the final step of deposition of PQT-12 to achieve the surface uniformity. The PQT-12 coated ITO substrate is annealed under an ambient environment at the glass transition temperature 140^oC (Sun *et al.*, 2009) which is then cooled down slowly at the rate of 2^oC/min. The final thickness of the PQT-12 layer is measured to be ~260 nm using reflectometer (F-20, Filmetrics). The prepared solution of colloidal CdSe QDs is then deposited on the PQT-12 coated ITO substrates and heated at 80^oC. It may be mentioned that we have used the same solvent chloroform for preparing the colloidal CdSe QDs as used for the PQT-12 solution. Note that the PQT-12 deposited at glass transition temperature has a very minimal solubility in chloroform which ensures that PQT-12 is not mixed with the colloidal CdSe QDs while depositing the CdSe QDs layer on the PQT-12 film by the spin-coating method. Furthermore, the spin-coated CdSe QDs layer is coated with the ethanedithiol for introducing the Mid-Gap Band (MGB) to improve the conductance of the CdSe QDs as mentioned in chapter 2. The process is repeated multiple times to achieve the desired thickness (~50 nm) of CdSe QDs measured using reflectometer (F-20, Filmetrics). Afterward, using the shadow mask technique, Au metal contacts (of ~80 nm thickness and 0.075 cm^2 area) are deposited on the CdSe QDs layer by a thermal evaporation method (HHV, FL400 SMART COAT 3.0 A). Thermal deposition of the Au electrode is performed with the deposition rate of 1.00 Å/s at a vacuum of ~10^{-6} bar. The complete fabricated device is shown in Figure 5.1 (b).

5.3 Result and Discussion

The current density- voltage (J-V) characteristics under dark and illuminated conditions of the hybrid PD is shown in Figure 5.3 (a) in both linear and log scales (inset). A white LED with an optical power density of 96 µW/cm^2 at 500 nm is used as the light source.

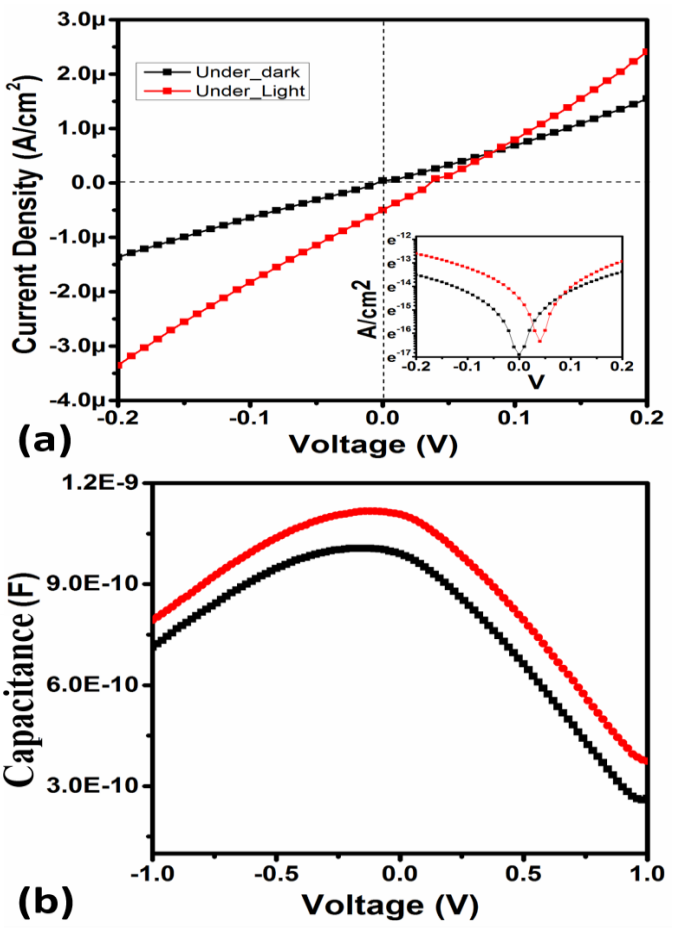

Figure 5.3: (a) Current density- voltage relationship of PQT-12/CdSe QD based hybrid self-powered photodetector under dark and light, inset shows the log plot, (b) Capacitance of the self-powered hybrid photodetector under the dark and illumination condition (96 µW/cm^2 at 500 nm).

Figure 5.3 (a) shows an open circuit voltage, V_{oc}, under illumination which forward biases the Au/CdSe Schottky junction to reduce its depletion region as:

$$W = \sqrt{\frac{2\varepsilon_s(\phi - V_{oc} - V)}{qN_d}} \tag{5.1}$$

where ϕ is the built-in potential, V is the bias voltage, $\mathcal{E}_s$ is the dielectric constant of the CdSe QDs, and N_d is the donor concentration of the CdSe QDs. The reduction in W increases the junction capacitance of the PD as shown in the measured capacitance-voltage (C-V) characteristics of the hybrid PD under dark and illuminated conditions at a frequency of 1 MHz in Figure 5.3 (b). The increased capacitance increases the potential energy ($E = 1/2 \times (C \times V^2)$) stored in the junction capacitance which allows the hybrid PD to work without any external source and behave as a self-powered hybrid PD. To investigate the response characteristics of the device, the measured transient response of PD is shown in Figure 5.4 at 0 V bias under illumination of white LED light in the form a pulse train with an ON-OFF period of 1 sec obtained by designing an Arduino™ based micro controller circuit.

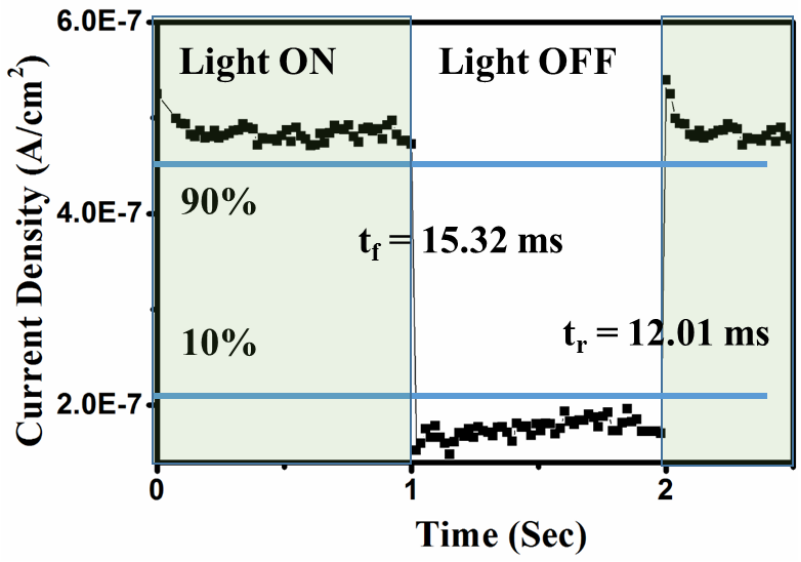

Figure 5.4: Time response characteristics under the pulsating LED light (96 µW/cm^2 at 500 nm) for an ON-OFF period of 1 sec.

The hybrid PD under study shows a rise time of ~12.01 ms and a fall time of ~15.32 ms which is faster than the results reported by Xie et al. (Xie *et al.*, 2013) and

Bera et al. (Bera *et al.*, 2016). The excess photogenerated carriers in the fully depleted CdSe QDs layer by Au/CdSe QDs and CdSe QDs/PQT-12 (C. Kumar *et al.*, 2017) junctions are quickly separated out by the electric field to result in the sharp rise of photocurrent as shown in Figure 5.4. The complete band diagrams of both junctions under dark and illumination are shown in Figure 5.5 (a) and (b), respectively.

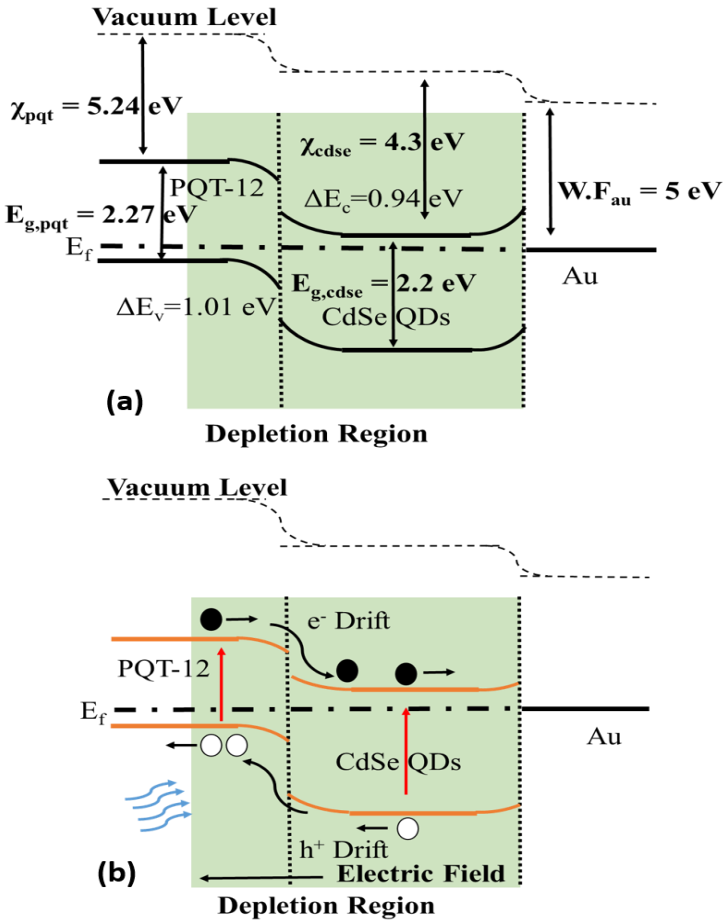

Figure 5.5: Schematic of the band energy diagram of CdSe QDs with PQT-12 and Au electrode (a) under thermal equilibrium or dark condition (b) under the illumination of light.

The figure of merit parameters such as responsivity (R_e) and the detectivity (D^*) of the PD can be calculated using Equation 2.5 and Equation 2.6. The calculated responsivity and detectivity of the PD are shown in Figure 5.6 (a). The PD shows a

responsivity of ~3.3 mA/W at 420 nm under a low optical power density of 130 μW/cm^2 which is comparable to the result reported by Game et al. (Game *et al.*, 2014).

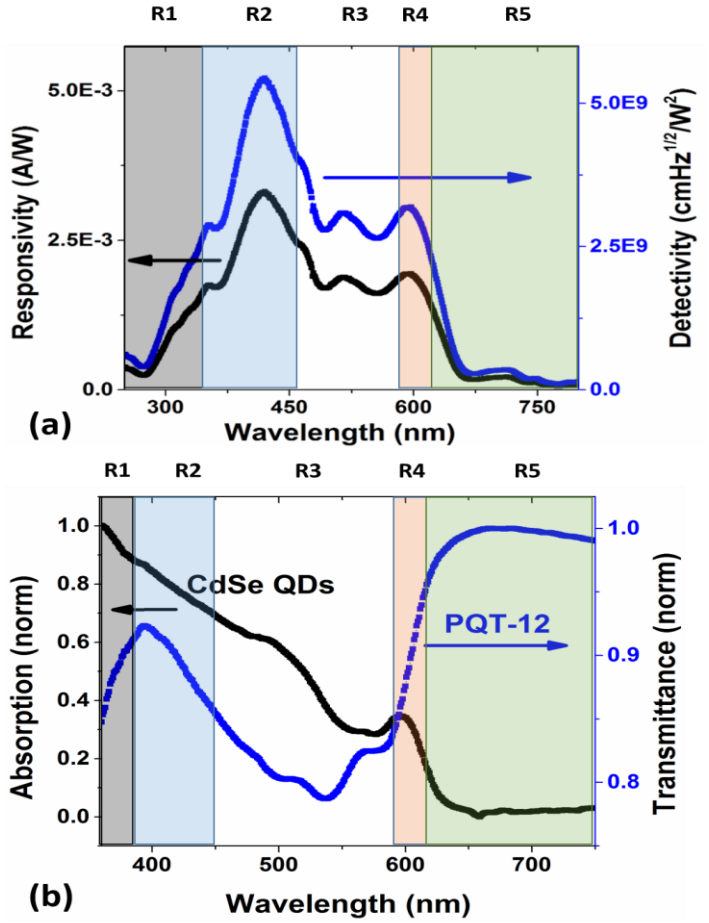

Figure 5.6: (a) Responsivity and detectivity of the hybrid self-powered photodetector at 0 V and (b) absorption and transmittance of CdSe QDs and PQT-12 respectively.

Note that Game et al. (Game *et al.*, 2014) achieved the responsivity of 6 mA/W at 470 nm under a very high optical power density of 18 mW/cm^2. Further, they fabricated their detector at a much higher temperature (>300°C) than that of our device. We have obtained a detectivity of 5.4x10^9 cmHz$^{1/2}$W^{-1} at 420 nm which is considered to be high enough to sense very weak light signals. Our detector parameters have been compared with those reported by others in Table 5.1. We will now investigate the effects of a PQT-12 layer on the optical characteristics of CdSe QDs layer. The photoluminescence

excitation and emission characteristics of the CdSe QDs have already been discussed in chapter 4 to demonstrate the synthesis of high quality and monodisperse CdSe QDs by the solution processed method considered in this study.

Table 5.1: Comparison of device response/photoresponse between the other related hybrid self-powered photodetectors.

Entities	p-type material	n-type material (Temperature)	Responsivity (A/W)	Detectivity ($cmHz^{1/2}W^{-1}$)	Illumination density	Rise Time/ Decay Time
(Xie *et al.*, 2013)	Spiro-MeoTAD	TiO_2 (500°C)	0.01 at 410 nm	--	75 µW/cm^2	0.12 Sec/ 0.06 sec
(Game *et al.*, 2014)	Spiro-MeoTAD	ZnO –N (450°C)	0.006 at 470 nm	--	18 mW/cm^2	4 ms/ 10 ms
(Bera *et al.*, 2016)	Spiro-MeoTAD	Sb_2S_3 (450°C)	0.087 at 475 nm	--	1.82 mW/cm^2	25 ms/ 25 ms
This Work	PQT-12	CdSe QDs (80°C)	~0.0033 at ~420 nm	$5.4x10^9$	130 µW/cm^2	15.32 ms/ 12.01 ms

The complete optical response of our PD can be distributed in five regions: *R1* (<390 nm), *R2* (391 to 450 nm), *R3* (451 to 590 nm), *R4* (591 to 610 nm), and *R5* (>611 nm) which can be explained in three following steps:

(i) The PD studied in the present study is a back-illuminated device. Hence the active layer (CdSe QDs) response is dependent upon the transmittance of filter layer

(i.e. PQT-12) as shown in Figure 5.6 (b). The transmittance of PQT-12 decreases in regions *R1* and *R3* whereas it is increased in *R2*, *R4*, and *R5*.

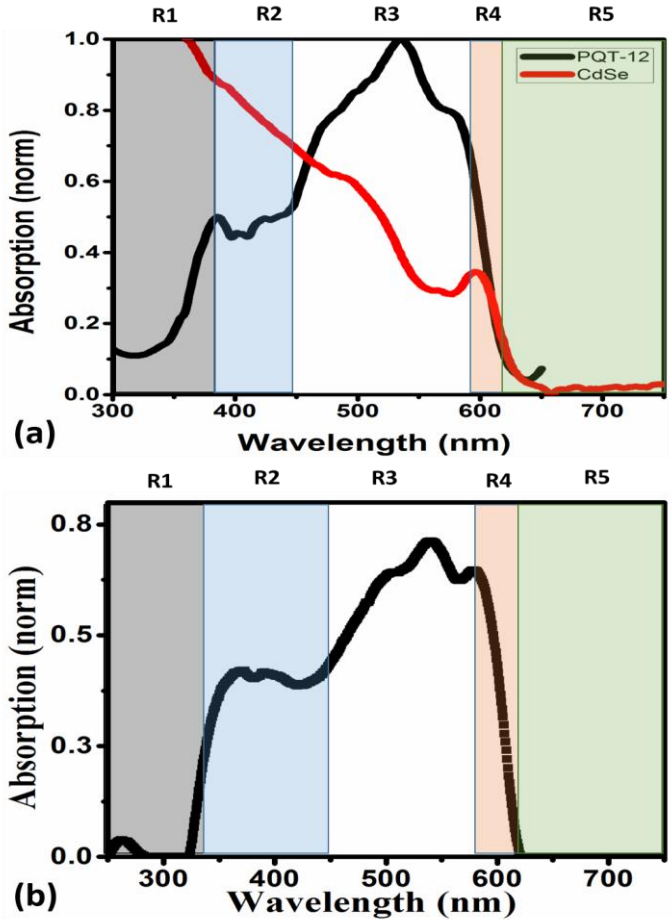

Figure 5.7: (a) Absorption profile of both CdSe QDs and PQT-12 and (b) complete absorption of PQT-12/CdSe QDs based self-powered hybrid detector.

(ii) The absorption of the active layer (CdSe QDs) starts from *R4* region and continuously increases in *R3*, *R2*, and *R1*. It is evident from Figure 5.6 (b) and Figure 5.7 (a) that the region *R2* will be the dominant spectral absorption region in active layer with the negligible absorption in the regions *R1* (short wavelength region) and *R5* (higher wavelength region).

(iii) The absorption characteristics of the complete device in Figure 5.7 (b) shows the bandpass characteristics of the complete PD under study with region *R1* and *R5* as

lower and upper limits respectively. The maximum absorption is achieved in *R3* due to the combined effects of PQT-12 and CdSe QDs whereas the device absorption achieved in *R2* is mostly due to the CdSe QDs.

The results are in line with the photoresponse achieved in Figure 5.6 (a) where the incident photons in the shorter wavelength region (*R1)* and higher wavelength region (*R5)* are observed to be nearly non-responsive. Further, the difference in the values of region R1 in Figure 5.6 (a) and Figure 5.7 (b) may be attributed due to the reflection from the Au electrode which is not considered in Figure 5.7 (b). Thus, the maximum values of photoresponse parameters R_e and D^* are achieved at 420 nm lying in the region *R2* mainly due to the CdSe QDs active region. The self-generated voltage V_{oc} under illumination discussed in Figure 5.3 (a) is responsible for working of this hybrid PD under study. Our proposed self-powered ITO/PQT-12/CdSe QDs/Au hybrid PD works in the visible region. The device shows the band-pass filter characteristics due to the combined effects of the CdSe QDs and PQT-12 films with a very sharp cut-off for higher wavelengths greater than 610 nm.

5.4 Conclusion

In this chapter, ITO/PQT-12/CdSe QDs/Au self-powered hybrid PD is fabricated and characterized where the colloidal CdSe QDs layer (inorganic) is used as the active layer deposited at a very low temperature ~80°C, and a PQT-12 thin film (polymer) prepared at glass transition temperature has been used as the filter layer of the device. The maximum responsivity and detectivity of hybrid self-powered PD are ~3.3 mA/W and 5.4×10^9 $cmHz^{1/2}W^{-1}$, respectively at ~420 nm under the incident optical power density of 130 $\mu W/cm^2$. The achieved responsivity and detectivity of the hybrid self-powered PD is lower compared to inorganic self-powered PD as discussed in chapter 4.

The hybrid self-powered PD gives the rise time and fall time of ~12.01 ms and ~15.32 ms respectively, which are much smaller than Au/CdSe QDs/ZnO QDs based self-powered PD discussed in chapter 4 due to the Au/CdSe QDs and CdSe QDs/PQT-12 dual junctions on both sides of the active CdSe QDs layer.